Wind profiles and low-level jet structures over the coastal waters of Japan

Kazutaka Goto[1,2], Takanori Uchida[3], Keisuke Nakao[1]

[1]Sustainable System Research Laboratory, Central Research Institute of Electric Power Industry, Chiba, 270-1194, Japan
[2]Interdisciplinary Graduate School of Engineering Sciences, Kyushu University, Fukuoka, 816-8580, Japan
[3]Research Institute for Applied Mechanics (RIAM), Kyushu University, Fukuoka, 816-8580, Japan

Correspondence to: Kazutaka Goto (ka-goto@criepi.denken.or.jp)

Abstract. Accurate characterization of coastal wind conditions is essential for offshore wind energy development; however, atmospheric structures in Japan's nearshore regions remain poorly understood. This study analyzed year-long vertical light detection and ranging (LiDAR) observations at closely located onshore and offshore sites along the Aomori coast to clarify the differences in wind profiles and their seasonal and directional dependence. Offshore wind speeds showed strong correlations ($r > 0.8$) with onshore data, indicating that, although direct substitution is inappropriate, onshore observations can effectively serve as reference data for offshore extrapolation when using the measure–correlate–predict (MCP) method. Low-level jets (LLJs) were more frequently observed under wind directions parallel to the coastline, with occurrence rates of 12–29% for southerly winds (SW–SE) and 8 %–10 % for northerly winds (N–NE), compared to other directions. The fraction of days with LLJ occurrences was also higher in spring and summer, reaching about 40 % in MAM and 37 % in JJA. Case analyses revealed that diurnal transitions associated with land–sea breeze circulation modulate vertical mixing and surface friction, promoting the development of LLJs. These results advance our understanding of nearshore boundary-layer dynamics and provide a basis for improving assessments of offshore wind resources, turbine designs, and LLJ forecasting strategies.

1 Introduction

The importance of renewable energy continues to increase due to constraints on fossil fuel supplies and the effects of global warming (Zecca and Chiari, 2010; REN21, 2024). In the future, offshore wind power is expected to become one of the primary sources of electricity generation (IEA and Wind, 2022). Wind conditions play a vital role in multiple aspects of offshore wind projects. For example, annual wind speeds must be incorporated during the planning stage of offshore wind power to ensure that suitable locations are selected and to accurately assess project viability (Bailey et al., 1997). We must also understand real-time wind speed during the operational stage of power stations because it directly affects the variability and uncertainty of wind farm electricity generation (Ward et al., 2023). However, in turbine load design, wind speed, turbulence intensity, wind shear, and veer must also be considered (Lundquist, 2022). The spatiotemporal distribution of inflow wind conditions is important to consider when evaluating turbine wakes (Lundquist, 2022; Porté-Agel et al., 2020), and wind speed influences scheduling maintenance vessel departures for operation and maintenance (O&M) activities (Si et al., 2025). Various studies

have been conducted to better elucidate offshore wind conditions, particularly in Europe (Dörenkämper et al., 2015; Schulz-Stellenfleth et al., 2022; Wagner et al., 2019). These studies have helped refine methods for evaluating offshore wind conditions (e.g., the appropriateness of using the power law to represent wind speed distributions) and improve wind forecasting techniques.

In general, a power law describes the vertical distribution of wind speed, with the exponent determined by land use. However, in offshore environments, wind speed does not always increase monotonically with height as expected, and in many cases, the power-law model is not applicable (Goto et al., 2025). The occurrence of low-level jets (LLJs) is a prominent example of this deviation (Dörenkämper et al., 2015; Schulz-Stellenfleth et al., 2022; Wagner et al., 2019). In coastal regions, land-sea interactions shape wind conditions, leading to complex boundary-layer dynamics. These interactions contribute to the development of phenomena such as LLJs. For example, Dörenkämper et al. (2015) used observational data from FINO2 in the Baltic Sea (Deutscher Wetterdienst, n.d.) and found that the formation of stable stratification over the ocean plays a significant role in LLJ development. Wagner et al. (2019) used FINO1 data from the North Sea and showed that LLJ formation is governed by multiple mechanisms, including baroclinicity associated with differential land–sea heating and frontal systems, as well as inertial oscillations induced by frictional decoupling. Various other coastal wind features have also been investigated. For instance, a reduction in surface friction can accelerate wind speed as wind flows from land to sea (Taylor, 1969). This acceleration also amplified the Coriolis force, resulting in a slight veering of the wind direction (Emeis et al., 2007). These findings exemplify the key features of coastal wind behavior relevant to offshore wind power development. However, the strong site-specific nature of wind conditions has necessitated continued research in this field. For example, local topography and climatic conditions can influence the occurrence of LLJs in coastal regions (de Jong et al., 2024; Qiu et al., 2023; Soares et al., 2022).

The terrain and climate in Japan differ markedly from those in Europe, where most previous research has been concentrated. Furthermore, offshore wind projects in Japan are often characterized by shorter fetches owing to the limited extent of shallow coastal seas, resulting in unique operational conditions (Renewable Energy Institute, 2021). Understanding the wind behavior under such distinct conditions is vital for advancing offshore wind energy in Japan; however, existing studies are limited in scope (Goto et al., 2025; Konagaya et al., 2021; Shimada et al., 2018). Shimada et al. (2018) explored the relationship between fetch length and wind-speed acceleration using two vertical-profiling LiDARs, and Konagaya et al. (2021) conducted statistical analyses of observational data from coastal land–sea regions. The authors investigated how wind direction, seasonality, and other factors affected variations in the wind speed exponent, mean wind speed, turbulence intensity, and related characteristics. These studies offer valuable insights into coastal wind conditions in Japan. However, as these analyses are primarily based on statistical approaches, they do not explicitly focus on individual meteorological events. As a result, event-based phenomena such as LLJs or monotonic shear—which affect offshore wind projects in other regions (Debnath et al., 2021; Schulz-Stellenfleth et al., 2022)—have not been fully characterized. Goto et al. (2025) used UAV observations to report the rapid development of stable stratification in nearshore areas and vertical wind profiles that the power law could not adequately capture. However, the underlying mechanisms remain unclear.

To address this research gap, this study investigated atmospheric structures in Japan's coastal regions using observational data from vertically profiled LiDARs installed on both onshore and offshore platforms. This study aimed to advance offshore wind energy in Japan by improving our understanding of coastal wind behavior. Statistical analysis was performed to identify the differences between onshore and offshore wind speeds, seasonal and directional variations in vertical wind profiles, and the occurrence characteristics of LLJs. Furthermore, we conducted detailed case analyses of selected LLJ events to clarify their formation mechanisms in the coastal environment.

2 Observations and methodology

2.1 Observation overview and setup

The vertical atmospheric structure was analyzed using observational data collected along the coast of Rokkasho in Kamikita District, Aomori Prefecture, Japan. The data were obtained from observation sites developed under a national research project by the New Energy and Industrial Technology Development Organization (NEDO). Notably, the dataset contributed to the development of the Offshore Wind Measurement Guidebook (NEDO, 2023) published by the NEDO, which is regarded as a highly reliable observational resource.

The surrounding environment and instrument locations are shown in Fig. 1. This figure also shows the onshore and offshore observation points used in this study. Offshore wind development areas in Japan are designated by the national government along both the Sea of Japan and the Pacific Ocean coasts. A sea area south of the study site (off Kuji City, Iwate Prefecture) has also been designated as a preparation zone, indicating that this coastal region is representative of ongoing offshore wind development in Japan. At the study site, the distance between the onshore and offshore observation points was approximately 1.6 km. Although floating offshore wind is being promoted in Japan, many projects remain located in nearshore waters. Therefore, a fetch of 1.6 km represents realistic nearshore wind conditions rather than an exceptional case. The surrounding area is flat and free of tall structures or complex terrain, thus minimizing the influence of local topography. The elevation of the onshore site was approximately *8* m a.s.l., resulting in a minimal height difference when compared with the offshore site.

Details for each observation point are listed in Tables 1 and 2. Each site was equipped with a measurement mast and a vertical profiling LiDAR. It should be noted that the measurement heights of the ZX300M LiDAR installed offshore varied depending on the observation period. The number of valid data points available for each height varied seasonally.

For both onshore and offshore sites, the vertical profiling LiDAR data consisted of 10-min average values recorded at 10-min intervals. Low-availability data segments were excluded from the analysis to ensure quality and consistency. An ultrasonic anemometer mounted on the measurement mast recorded the wind data at a sampling frequency of 10 Hz. All subsequent analyses of the observational data were conducted using these 10-min averaged values at 10-min intervals.

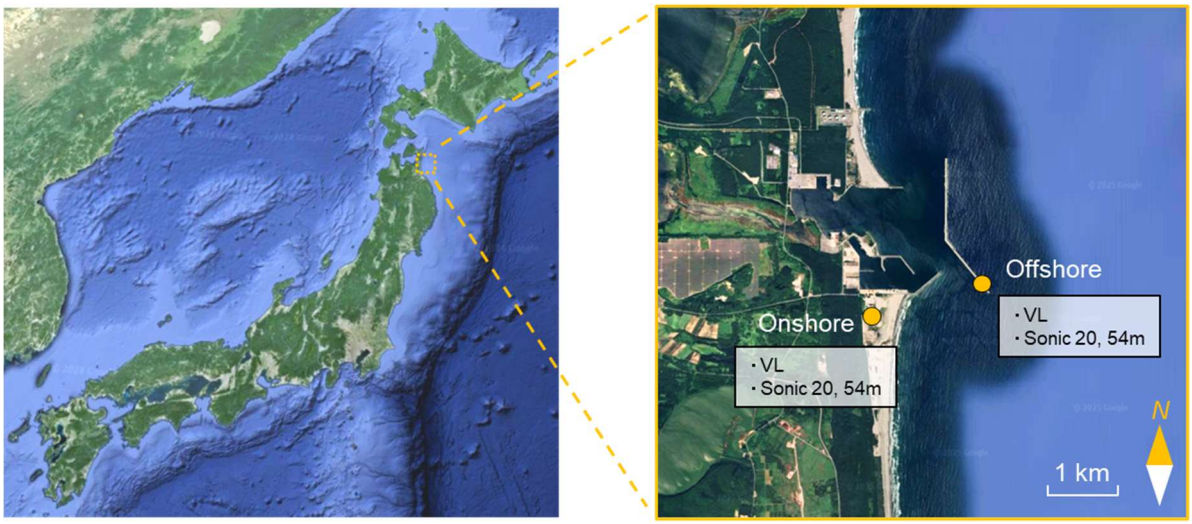

Figure 1: Observation sites and the surrounding environment. VL indicates vertical light detection and ranging (LiDAR). Observation sites are the coast of Rokkasho in Kamikita District, Aomori Prefecture, Japan. The offshore measurements were conducted on a breakwater. Background map data: © 2024 Google (left) and © 2025 Google (right).

Table 1: Onshore observational setup

	Period	Interval	Data type	Height above land surface	Instruments
Vertical profiling LiDAR	01/09/2023–31/08/2024	---	*10*-min average	*40, 45, 50, 54, 58, 60, 70, 80, 90, 100, 110, 120, 130, 140, 150, 160, 180, 200, 250, 300* m	Windcube v2.1 (Vaisala; developed initially by Leosphere, France)
Ultrasonic anemometer	01/09/2023–31/08/2024	*10* Hz	*10* Hz	*20, 54* m	SAT-900 (Sonic Corporation, Japan)

Table 2: Offshore observational setup

	Period	Interval	Data type	Height above sea surface	Instruments
Vertical profiling LiDAR	01/09/2023–30/11/2023	*1* Hz	*10*-min average	*25, 53, 63, 100, 115, 130, 160, 250, 300* m	ZX300M (ZX lidars, UK)
	01/12/2023 – 29/02/2024			*25, 53, 63, 100, 115, 130, 160, 250, 300* m	
	28/03/2024–31/05/2024			*25, 53, 63, 100, 120, 130, 150, 160, 180, 240* m	
	07/06/2024–31/08/2024			*25, 53, 63, 86, 107, 120, 150, 180, 240* m	
Ultrasonic anemometer	01/09/2023–31/08/2024	*10* Hz	*10* Hz	*25, 59* m	SAT-900 (Sonic Corporation, Japan)

2.2 Low-level jet detection

LLJs are among the most prominent coastal atmospheric phenomena influencing offshore wind conditions. Their formation mechanisms are diverse and have been studied extensively in previous literature (Dörenkämper et al., 2015; Schulz-Stellenfleth et al., 2022; Wagner et al., 2019). However, no study has specifically addressed LLJs in the context of offshore wind energy development in Japan. Consequently, their occurrence, causes, and characteristics in Japanese coastal regions remain poorly understood. In particular, the relatively short offshore fetch, which is characteristic of offshore wind conditions in Japan, may play a role in LLJ formation.

As highlighted by Hallgren et al. (2023), there is currently no consensus on a definition of LLJ, and the development of appropriate identification criteria is ongoing. The diversity in LLJ structures observed across regions and meteorological regimes has contributed to the lack of standardization. Thus, to investigate LLJs in this study, it was essential to first define them.

In this study, LLJs were identified using two sets of criteria depending on the objective. First, for comparison of LLJ occurrence rates with European cases, the detection criteria proposed by Wagner et al. (2019) were applied, as expressed in Eq. (1).

$$u_{max} - u_{min} \geq 2\ m\ s^{-1} \wedge u_{max} \geq 1.25\ u_{min}\ , \tag{1}$$

The definitions of the local maximum wind speed u_{max} and the local minimum wind speed u_{min} are illustrated in Fig. 2. If no local minimum is identified above the local maximum, the wind speed at the highest available measurement height is used as umin. These thresholds are designed to avoid false detections under both low and high wind speed conditions.

Next, to investigate offshore wind structures characterized by low-level wind speed maxima, LLJs were extracted using a modified criterion, as shown in Eq. (2).

$$u_{max} \geq 4\ m\ s^{-1} \wedge u_{max} \geq 1.1\ u_{min}, \tag{2}$$

The threshold of 4 m s^{-1} in Eq. (2) corresponds to the cut-in wind speed of typical wind turbines. Under the criterion of Eq. (1), even if a low-level wind speed maximum is present, it cannot be identified as an LLJ unless a corresponding u_{min} satisfying the criteria exists. However, in the context of this study, such profiles are also considered valuable for analysis. Therefore, the relative threshold was relaxed to allow inclusion of profiles with relatively weak low-level wind speed maxima.

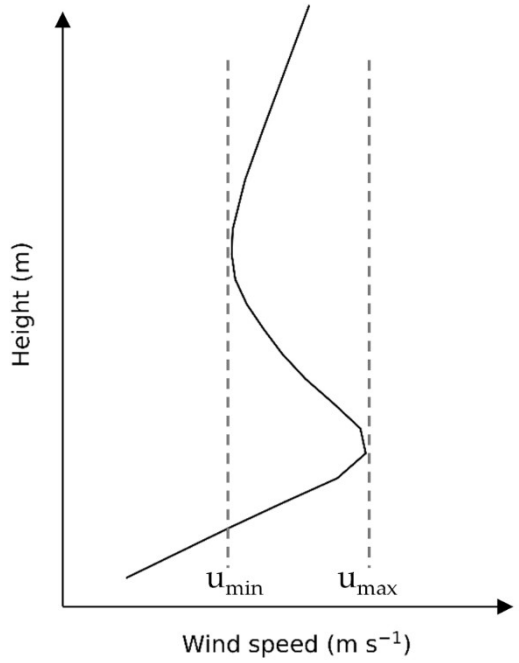

Figure 2: Schematic illustration of the identification of u_{min} and u_{max} from a vertical wind speed profile. u_{max} represents the local maximum wind speed (jet core), while u_{min} denotes a local minimum in the profile used for LLJ detection.

2.3 Atmospheric stability evaluation

Atmospheric stability is indispensable when analyzing wind conditions in the atmospheric boundary layer, and is often quantified using the Monin–Obukhov length, L (Gryning et al., 2007). However, in this study, rather than directly using L as a stability index, we separately evaluate the friction velocity and the covariance $\overline{w'T'}$, which are used in the derivation of L based on the eddy covariance method (Stull, 1988), in order to better capture offshore atmospheric structure.

Several methods have been developed to estimate L, including the eddy covariance method and the bulk method (Grachev and Fairall, 1997). Although bulk methods exploit vertical gradients in meteorological variables between two levels, these approaches may not accurately represent local stability in oceanic regions, where vertical stratification is often non-uniform (Wagner et al., 2019). In contrast, the eddy covariance method allows estimation of local atmospheric stability from flux measurements at a single point.

In this study, high-frequency data from ultrasonic anemometers installed onshore and offshore were used to compute the friction velocity and the covariance $\overline{w'T'}$, which are used in the calculation of the Obukhov length based on the eddy covariance method. Prior to analysis, a tilt correction was applied to the ultrasonic anemometer data using the planar-fit (PF)

method (Wilczak et al., 2001). The regression coefficients (b_0, b_1, b_2) were determined daily using the linear relationship given by Eq. (3):

$$\bar{w}_m = b_0 + b_1\bar{u}_m + b_2\bar{v}_m\,, \tag{3}$$

where $\bar{u}_m$ and $\bar{v}_m$ are the mean horizontal wind speed components, and $\bar{w}_m$ is the mean vertical wind speed component, all of which are expressed in the instrument coordinate system. Following the approach of Wilczak et al. (2001), the regression coefficients were determined using 15-min averaged data collected each day. After applying tilt correction, the deviations from the mean were calculated for each wind and temperature component. These deviations were then used to compute the friction velocity and L as defined in Eqs. (4) and (5):

$$u_* = \left(\overline{u'w'}^2 + \overline{v'w'}^2\right)^{1/4}, \tag{4}$$

$$L = \frac{{u_*}^3}{\kappa\frac{g}{\bar{T}}\overline{w'T'}}\,, \tag{5}$$

where u_* denotes the friction velocity. The constants κ and g are the von Karman constant and gravitational acceleration, respectively, and T is the air temperature. Although L was calculated using the above equations, the offshore values of covariance $\overline{w'T'}$ were extremely small. As covariance $\overline{w'T'}$ appears in the denominator of Eq. (5), this led to unstable and spiky behavior in L. Therefore, rather than using the Obukhov length as a stability index, we directly examined friction velocity and covariance $\overline{w'T'}$ to better represent the vertical atmospheric structure.

3 Offshore wind conditions near the coast of Japan

3.1 Comparison of onshore and offshore wind speeds

This section focuses on characterizing the wind conditions at the study site by comparing onshore and offshore wind speeds. Based on the NEDO Wind Observation Guidelines (2023), wind speeds *120* m above the onshore and offshore areas were compared for *16* wind directions. The classification of wind direction was determined using *120* m wind direction data from the offshore Doppler LiDAR. The comparison of mean wind speeds by wind direction and season is shown in Fig. 3, while the correlation between 10 min averaged onshore and offshore wind speeds is presented in Fig. 4. Although the mean wind speeds shown in Fig. 3 exhibit no pronounced onshore–offshore differences, the correlation analysis based on 10 min averages (Fig. 4) reveals clear directional dependence. High correlations were observed under sea–breeze conditions, whereas low correlations were observed under land–breeze conditions. This trend is consistent with the findings of Konagaya et al. (2021) and can be attributed to differences in the surface roughness length. Specifically, under land breeze conditions, winds pass over inland areas with relatively high surface roughness, resulting in reduced onshore wind speeds. As the flow transitions offshore, where the roughness is lower, the wind speed increases, leading to a greater difference between the onshore and offshore wind speeds. In contrast, under sea-breeze conditions, winds primarily travel over the ocean and coastal areas, both

of which have relatively low surface roughness, allowing higher wind speeds to be maintained, even onshore. Consequently, the difference between the onshore and offshore wind speeds tends to be smaller. Furthermore, for wind directions other than land and sea breezes, particularly those parallel to the coastline (N and S), the correlation was lower than that for land breezes. A comparison of wind speeds between onshore and offshore sites revealed that the data did not meet the criteria specified in the NEDO guidelines (2023), indicating that onshore wind speed data should not be used directly as a substitute for offshore data. However, this does not preclude the use of onshore data in measure–correlate–predict (MCP) applications. The MCP method is commonly used to supplement missing wind observations by correlating data from nearby sites; for example, by using onshore data to estimate offshore conditions. In this context, a correlation coefficient of approximately 0.8 or higher is generally considered acceptable (Carta et al., 2013), and this criterion was satisfied in the present analysis. Therefore, for coastal locations with short offshore distances, such as those examined in this study, the MCP method based on onshore wind data appears to be a valid and effective approach for estimating offshore wind conditions.

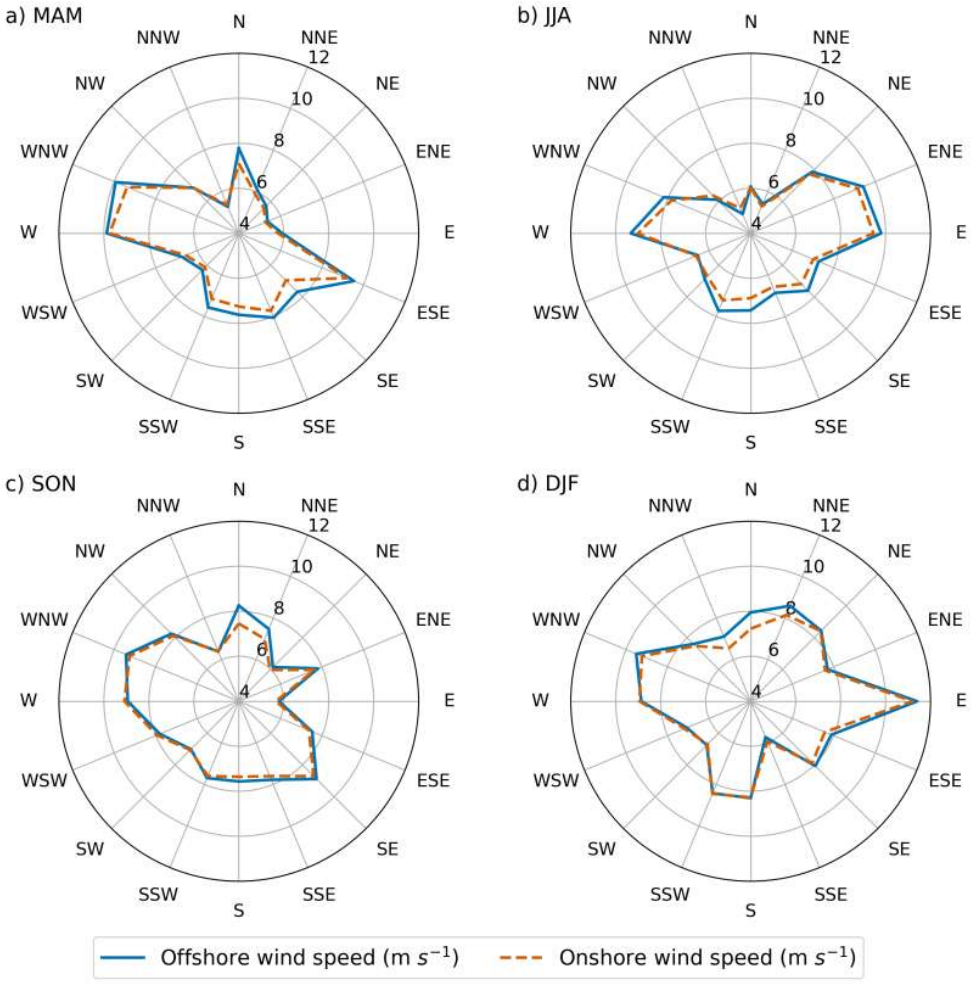

195 **Figure 3: Comparison between onshore and offshore mean wind speeds by wind direction and season at 120 m height. Wind direction labels follow meteorological convention (e.g., N = north, WNW = west-northwest). Seasons are abbreviated as MAM (March-May), JJA (June-August), SON (September-November), and DJF (December-February).**

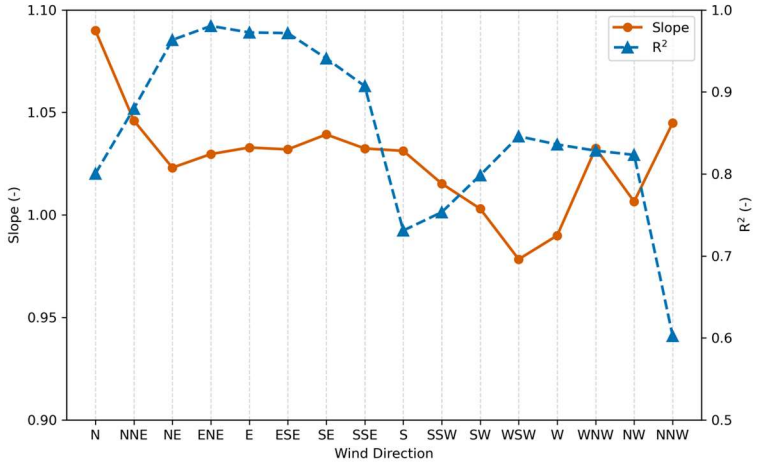

Figure 4: Correlation between onshore and offshore 10-min averaged wind speeds by wind direction at 120 m. Wind direction labels follow meteorological convention (e.g., N = north, WNW = west-northwest).

The vertical profiles of the normalized wind speed were averaged by wind direction and season (Fig. 5). The normalized wind speed was defined as the wind speed at each height divided by the wind speed at the highest available measurement height for each profile. The normalization was applied to each individual profile prior to averaging. Since the available measurement heights differed among seasons, the reference height used for normalization varied accordingly for each season (Table 1 and 2). This normalization allows comparison of vertical structures independent of absolute wind-speed magnitude. In Fig. 5, representative wind directions were selected based on the four cardinal directions. As shown in Fig. 1, the upwind geographical conditions differ between the northwesterly and southwesterly sectors within the westerly flow. Therefore, the westerly direction was subdivided into WNW and WSW for comparison. In autumn and winter, and for land-breeze directions (WNW and WSW), the wind-speed differences between the onshore and offshore sites tended to be larger at lower altitudes. This behavior is consistent with the development of an internal boundary layer over the sea, driven by a change in the surface roughness length from land to sea; that is, wind speeds in the internal boundary layer increase. In addition, during spring and summer, wind directions parallel to the coastline (N and S) and sea breeze (E) often exhibited LLJ structures in the vertical profiles, with wind speeds at lower altitudes exceeding those at higher altitudes. A detailed analysis of this phenomenon is presented in the following subsections.

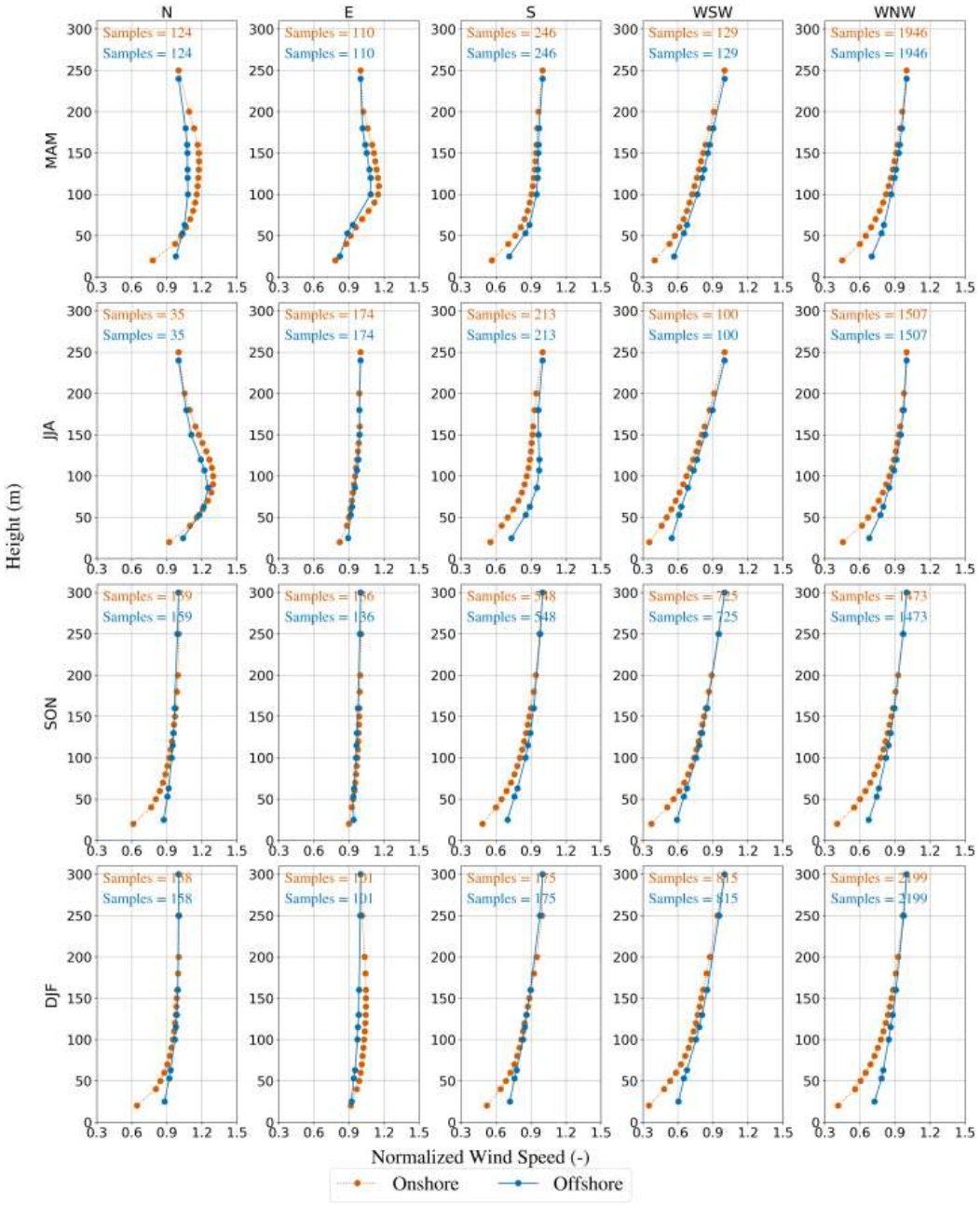

Figure 5: Vertical profiles of normalized wind speed averaged by wind direction and season. The normalized wind speed was defined as the wind speed at each height divided by the wind speed at the highest available measurement height for each profile. The normalization was applied to each individual profile prior to averaging. The sample size indicates the number of 10-min averaged data points that fall within each wind direction sector in the one-year dataset. Wind direction labels follow meteorological convention (e.g., N = north, WNW = west-northwest). Seasons are abbreviated as MAM (March-May), JJA (June-August), SON (September-November), and DJF (December-February).

3.2 Frequencies and characteristics of LLJs

LLJ detection was performed using 10-min averaged vertical wind profiles derived from Doppler LiDAR measurements. Based on Eq. (2) in Sect. 2.2, the frequencies of LLJ occurrences were calculated as a function of wind direction (Fig. 6). The frequency distribution shown in Fig. 6 indicates that WNW winds are dominant at this site, resulting in a large absolute number of LLJ cases in this direction. However, the highest relative occurrence rates were observed under SE winds. As indicated by the wind-direction-dependent LLJ occurrence rates, LLJ formation exhibits a strong directional dependence. In particular, higher occurrence rates were observed for southerly winds, followed by northerly winds. Although along-coast LLJs may sometimes be associated with terrain-induced mechanisms, such as those reported by Soares et al. (2022), the study site is not characterized by steep coastal topography. Therefore, the underlying mechanism at this site is likely to differ from terrain-blocking effects observed elsewhere. A more detailed analysis of the LLJ formation mechanisms is provided in the following section.

The seasonal variation of LLJ frequency was further examined (Table 3). Table 3 presents LLJ frequencies calculated using both Eq. (1) and Eq. (2). Since Eq. (2) uses a less restrictive criterion than Eq. (1), the occurrence rates derived from Eq. (2) are generally higher. It should be noted that the occurrence rates presented here are calculated relative to the total number of days, rather than the total number of 10-min interval records. LLJs were observed more frequently in spring and summer. This seasonal tendency is consistent with results from European studies focusing on the North and Baltic Seas (Dörenkämper et al., 2015; Schulz-Stellenfleth et al., 2022; Svensson et al., 2016; Wagner et al., 2019). For comparison with European studies, we used the LLJ frequencies calculated using Eq. (1), Wagner et al. (2019) reported daily LLJ occurrence rates of 74 %–81 % in spring and summer in the southern North Sea, whereas the present study indicates a lower daily occurrence rate of approximately 39 %. However, this comparison is based on a single observation site, and additional measurements across multiple locations in Japan are required to confirm the robustness of this finding. LLJs in the subsequent analysis are identified using Eq. (2). Under the criterion defined by Eq. (1), even when a low-level wind speed maximum is present, the profile is not classified as an LLJ unless a corresponding u_{min} criterion is also satisfied. In the context of this study, such profiles are considered physically meaningful and are therefore included in the analysis using the relaxed criterion.

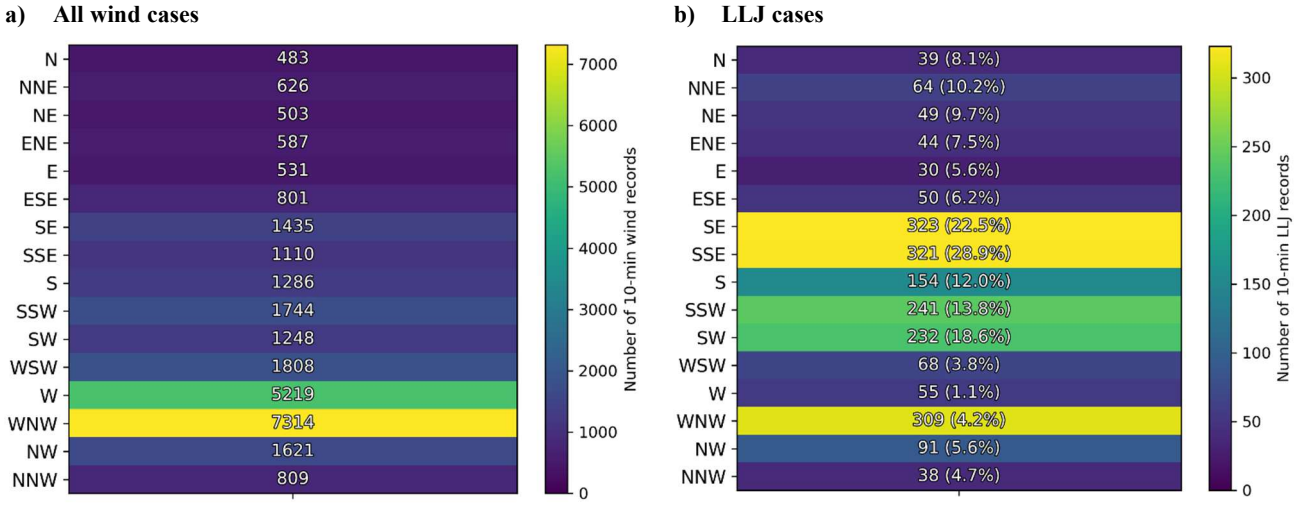

Figure 6: Frequencies of LLJs occurrences by wind direction. The color scales differ between panels. In panel (a), the values represent the number of 10-min wind records for each wind direction. In panel (b), values in parentheses indicate the LLJ occurrence rate (%), defined as the ratio of LLJ records to the total number of wind records for each direction. Wind direction labels follow the meteorological convention (e.g., N = north, WNW = west-northwest).

Table 3: Seasonal number of LLJ days

Season	Total analyzed days	LLJ days (Eq. (1), standard criterion)	LLJ days (Eq. (2), relaxed criterion)
MAM	*64*	*26 (40.6 %)*	*51 (79.7 %)*
JJA	*83*	*31 (37.3 %)*	*66 (79.5 %)*
SON	*91*	*11 (12.1 %)*	*44 (48.4 %)*
DJF	*88*	*10 (11.4 %)*	*38 (43.2 %)*

Values in parentheses represent the LLJ occurrence rate (%), defined as the ratio of LLJ days to the total number of valid days in each season. LLJ occurrence is counted if at least one LLJ event was detected within a day. Seasons are abbreviated as MAM (March-May), JJA (June-August), SON (September-November), and DJF (December-February).

To analyze the mechanisms of LLJ formation, the hour-of-day distribution of LLJ occurrences was examined by wind direction during spring and summer, when LLJs are observed more frequently (Fig. 7). As shown in Fig. 6, the LLJ occurrence frequency exhibits different tendencies among the four cardinal sectors. Therefore, one wind direction was selected from each sector (E, S, W, and N) for detailed analysis. As described in Sect. 3.1, the upstream characteristics differ between WNW and WSW within the westerly sector. In the present analysis, WNW was selected because it provides a larger number of LLJ samples. As shown in Fig. 7, LLJ occurrence exhibits a strong dependence on the hour of the day. Furthermore, peak occurrence times varied with wind direction. For example, E tended to peak immediately after noon, followed by S in the early evening. In contrast, N and WNW tended to peak at night, although N exhibited different trends in spring and summer. However, for the N wind direction, not only the number of LLJ samples but also the number of all samples is limited, and the distribution is uneven; therefore, this interpretation should be treated with caution. For the E wind direction, although the number of LLJ

samples is also small, similar trends are observed in spring and summer, and the number of all samples is larger than that for N and more evenly distributed. Therefore, a more reliable interpretation is possible for E compared to N. These findings suggest that the LLJ generation is closely related to the diurnal cycle. A more detailed discussion is provided in Sect. 4.

The maximum wind speeds during the LLJ events are shown in Fig. 8. LLJ core wind speeds exhibited some variability among wind directions; however, no single wind direction consistently dominated in terms of core wind speed. Importantly, the LLJ core wind speeds observed in this study were lower than those reported in Europe (Wagner et al., 2019) and the United States (Debnath et al., 2021). This indicates that LLJs over Japan may be characterized by relatively weaker wind speeds. However, it should be noted that this result was based on a single site. Therefore, future studies using additional observational data across multiple coastal locations in Japan are necessary to evaluate the effects of LLJ characteristics on offshore wind energy development (Hallgren et al., 2023).

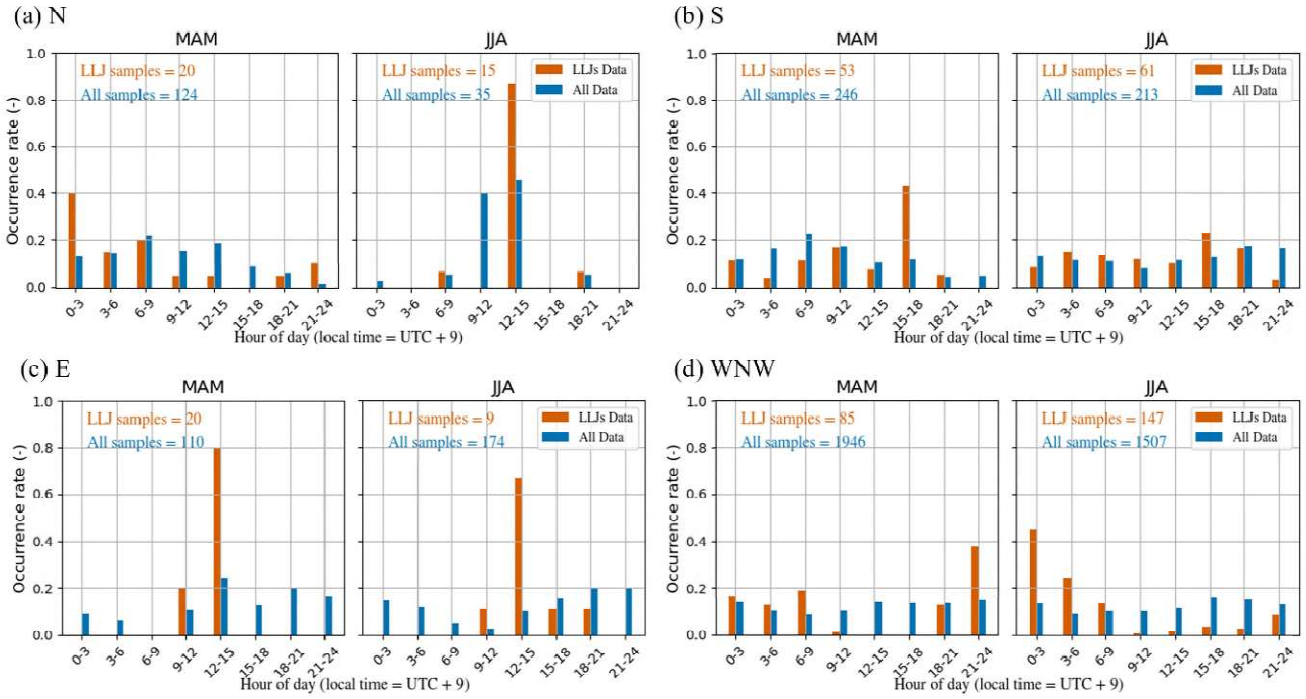

Figure 7: Hour-of-day distribution of LLJ occurrences. Wind direction labels follow meteorological convention (e.g., N = north, WNW = west-northwest). Seasons are abbreviated as MAM (March-May), JJA (June-August), SON (September-November), and DJF (December-February).

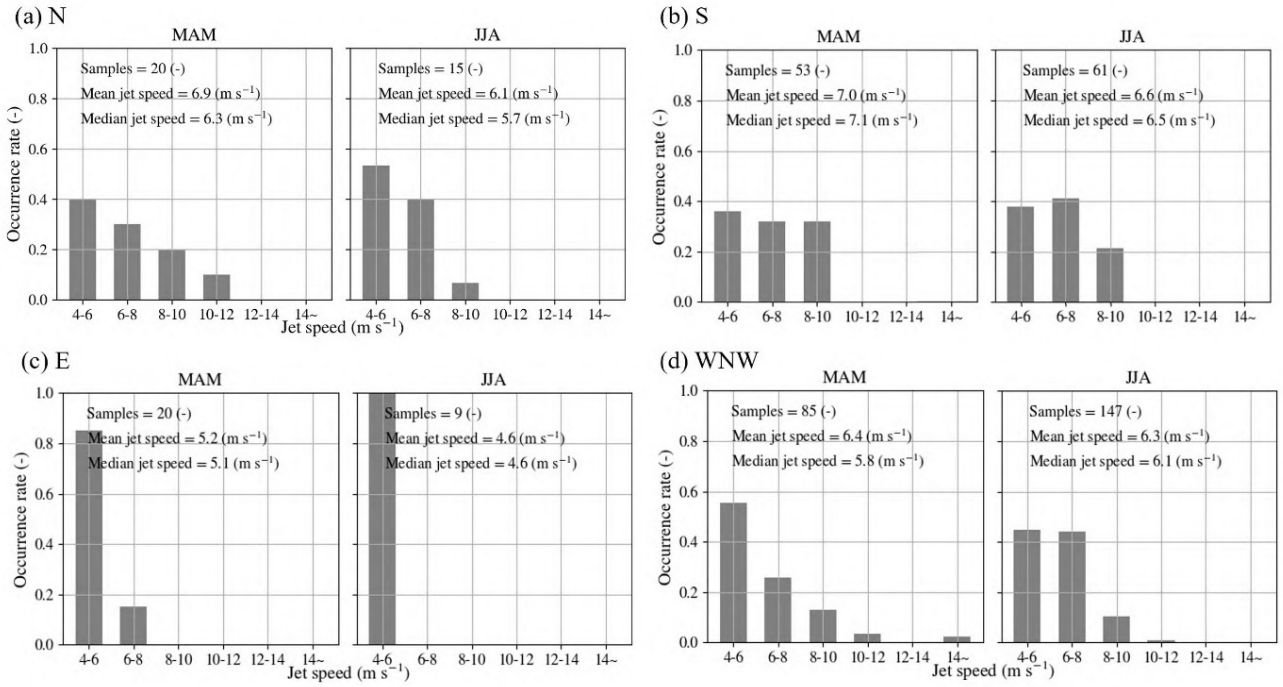

Figure 8: LLJ core wind speeds by wind direction in spring and summer. Wind direction labels follow meteorological convention (e.g., N = north, WNW = west-northwest). Seasons are abbreviated as MAM (March-May), JJA (June-August), SON (September-November), and DJF (December-February).

4 LLJ formation mechanism based on observational case studies

In Sect. 3 it was revealed that LLJs exhibit not only seasonal dependence, but also strong associations with specific wind directions and times of day. This directional and temporal regularity suggests a strong link between the LLJ formation and diurnal atmospheric cycles. Several representative LLJ formation mechanisms have been proposed in the literature, most notably those proposed by Blackadar (1957) and Holton (1967), both of whom attribute LLJ formation processes to diurnal cycles. This section provides an overview of selected observational cases during spring and summer to explore the relationship between LLJ formation and diurnal coastal processes.

Time series data for wind speed and direction on May 2, 2024, are shown in Fig. 9, as a representative case of LLJ occurrence under southeasterly (SE) wind conditions, together with the vertical profiles of wind speed including LLJ occurrence times in Fig. 10. In this case, a land breeze prevailed from nighttime to early morning, and the wind speed gradually decreased. This was followed by a transition to a sea breeze, representing a typical sea–land breeze circulation. As shown in Figs. 9 and 10, after this shift in the morning, the vertical relationship of wind speeds among different heights was reversed. Furthermore, in

the afternoon, the wind speed fluctuated while the wind direction gradually veered clockwise, transitioning from a sea breeze to southerly wind. As shown in Fig. 10, LLJ occurrence can be confirmed during this process. According to Fig. 7, the peak occurrence of LLJs under easterly conditions occurred between 12:00 JST (local time = UTC + 9 h) and 15:00 JST, followed by a peak under southerly conditions between 15:00 and 18:00 JST. This behavior is consistent with the clockwise rotation of the wind direction associated with the increase in wind speed observed on 2 May. Because Fig. 7 is based on statistical analysis, this clockwise rotation of wind direction is considered a typical feature. Before discussing these mechanisms in detail, we introduce another case of LLJ formation under the dominant wind direction (WNW) at the study site. A time series of wind speed and direction on July 11, 2024, is shown in Fig. 11, together with vertical profiles of wind speed at selected times in Fig. 12. In this case, wind speed increased from evening to nighttime, accompanied by a clockwise rotation of the wind direction. However, before the wind direction fully transitioned to northerly flow, the wind speed decreased, and the wind direction subsequently reversed to counterclockwise rotation. As shown in Fig. 12, an LLJ developed during the nighttime as wind speed increased, whereas no LLJ was observed around 04:00 when the wind direction shifted to counterclockwise rotation. These clockwise rotations in wind direction are consistent with the mechanism described by Blackadar (1957). According to this theory, the transition from a daytime mixed layer to nocturnally stable stratification reduces the friction layer, allowing upper-level winds to become decoupled from surface friction. Consequently, the wind speed increases, and the wind direction rotates clockwise owing to the action of the Coriolis force.

For the two representative LLJ cases described above, hodographs of the wind vector at 120 m offshore are shown in Fig. 13 to clearly illustrate the rotational behavior. Wind direction is influenced not only by the Coriolis force but also by pressure-gradient forces and surface friction; therefore, it does not necessarily exhibit a strictly monotonic clockwise rotation. Nevertheless, on a timescale of several hours, both cases show a tendency for the wind direction to rotate clockwise in association with an increase in wind speed. The rotation rate of the wind direction was estimated from the change in wind direction between the start and end points indicated in Fig. 13, divided by the corresponding time interval. To reduce the influence of short-term fluctuations, the wind directions at the start and end points were evaluated using unit-vector-averaged values based on three consecutive data points, including ±10 minutes. The Coriolis frequency is given by Eq. (6):

$$f = 2\Omega \sin\varphi \,, \tag{6}$$

where Ω is the Earth's angular velocity and φ is latitude. At the study site ($\varphi \approx 40.924°$) and with $\Omega = 7.292 \times 10^{-5}\ rad\ s^{-1}$, the Coriolis frequency is estimated as $f \approx 9.57 \times 10^{-5}\ s^{-1}$. Converting this frequency into an angular rotation rate yields a theoretical inertial rotation rate of approximately $19.7°\ h^{-1}$. The rotation rates of the wind direction estimated from the observations are approximately $14.4°\ h^{-1}$ on 2 May and $21.4°\ h^{-1}$ on 11 July, which are of the same order as the theoretical inertial rotation rate. These results provide quantitative support for the interpretation that the observed LLJs are governed by inertial oscillation following frictional decoupling, consistent with Blackadar's theory. As shown in Fig. 6, the occurrence rate of LLJs is higher under southerly and northerly wind directions. Furthermore, Fig. 7 indicates that LLJ occurrence tends to peak later in time under southerly winds compared to easterly winds, and under northerly winds compared to west-northwesterly winds (for

MAM only). These tendencies are consistent with the inertial oscillation mechanism. Specifically, following the wind-direction shift associated with the land–sea breeze circulation, inertial oscillations are initiated under easterly or westerly wind conditions. As wind speed gradually increases and the wind direction rotates clockwise, LLJs are more likely to develop when the wind vector evolves toward southerly or northerly directions.

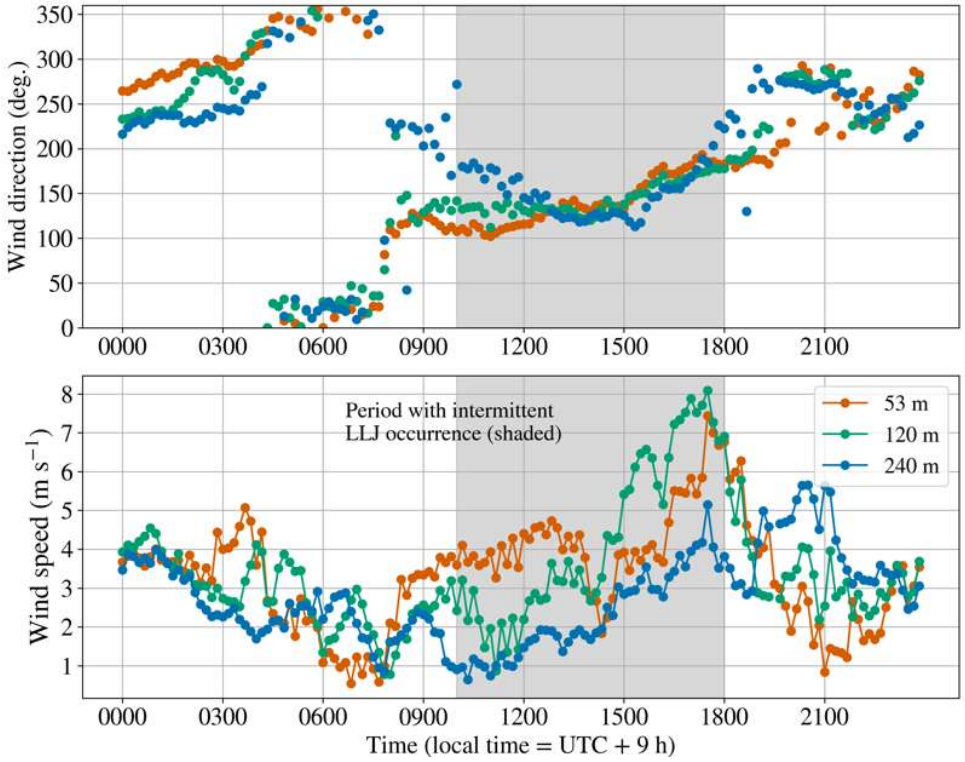

Figure 9: Time series of wind speed and direction on 2 May 2024. The legend indicates the observational height.

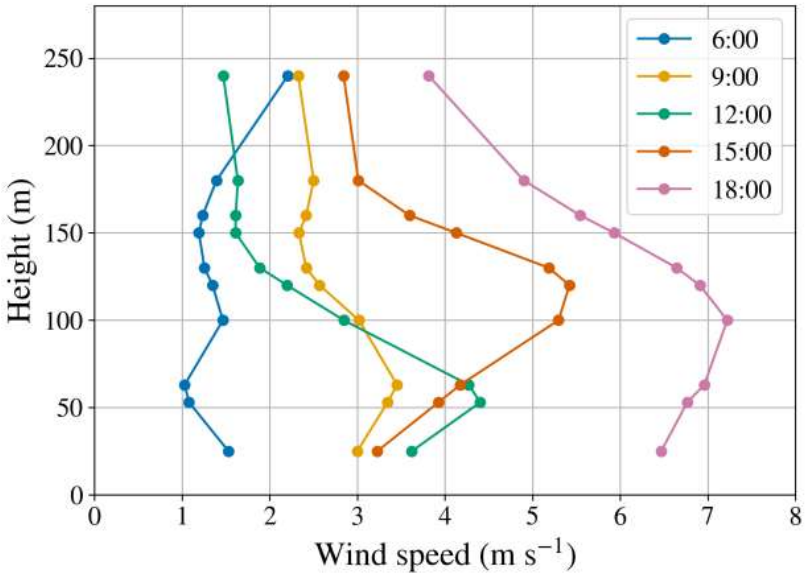

Figure 10: Vertical profiles of wind speed at selected times on 2 May 2024.

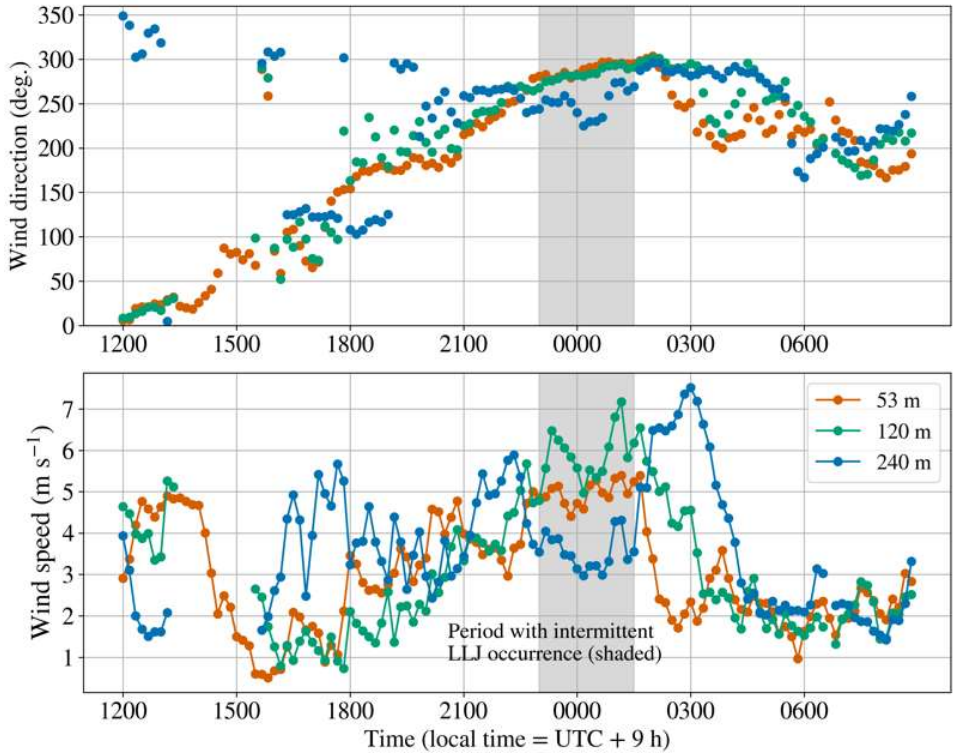

Figure 11: Time series of wind speed and direction on 11 July 2024. The legend indicates the observational height.

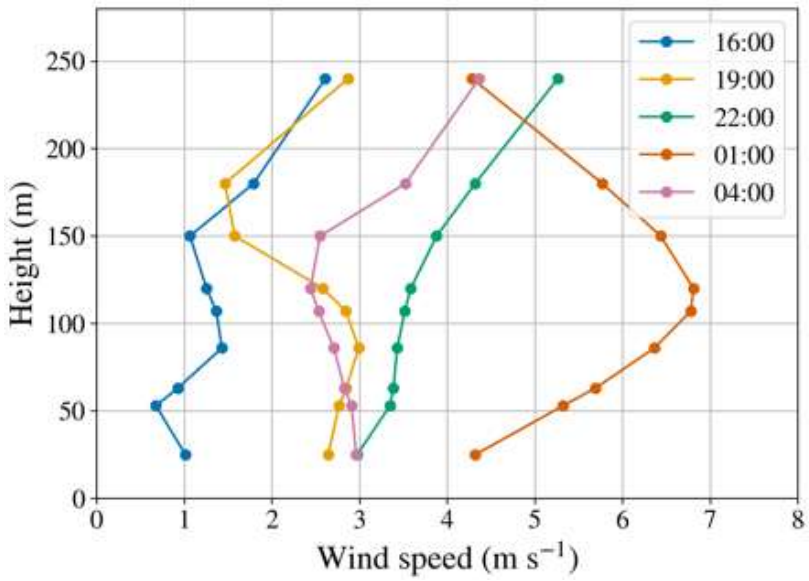

Figure 12: Vertical profiles of wind speed at selected times on 11 July 2024.

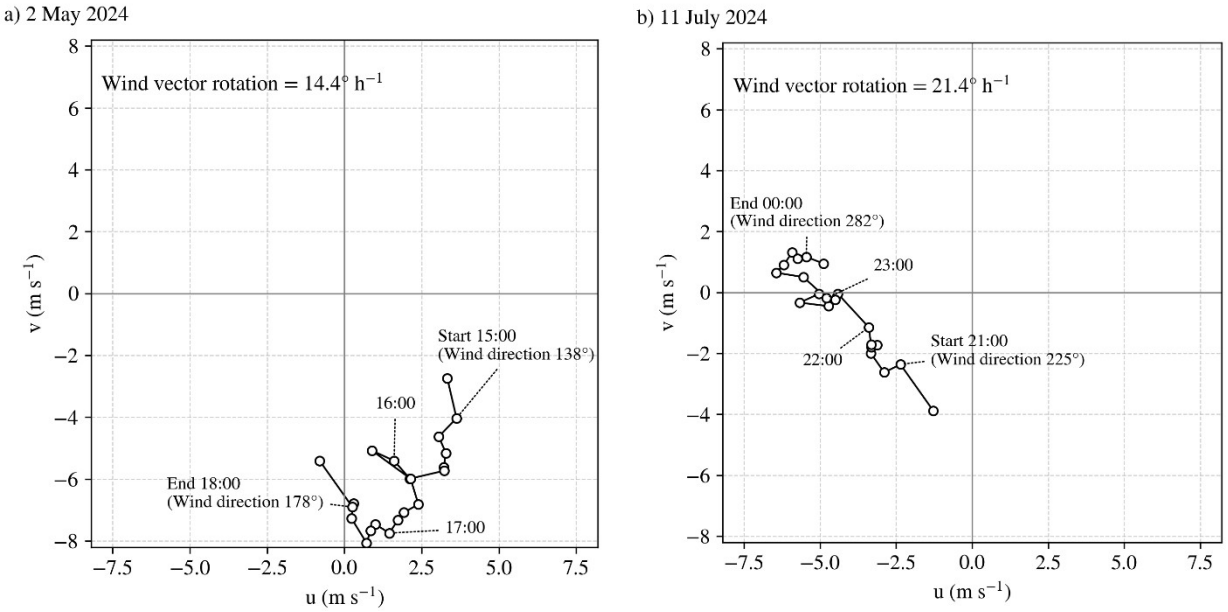

Figure 13: Hodographs of the wind vector at 120 m offshore. Panels (a) and (b) show representative LLJ cases on 2 May and 11 July 2024, respectively. The hodographs illustrate the temporal evolution of wind vectors, highlighting a clockwise rotation associated with increasing wind speed during LLJ development. The start and end points used to estimate the rotation rate are indicated. The estimated rotation rates are 14.4° h⁻¹ and 21.4° h⁻¹, respectively, which are comparable to the theoretical inertial rotation rate (19.7° h⁻¹) derived from the Coriolis parameter at the study latitude.

In this study, we interpreted the offshore LLJ formation mechanism observed on May 2 by integrating Blackadar's theory with the influence of sea–land breeze circulations. Figure 14 presents the time series of friction velocity u_* and covariance of vertical velocity and temperature ($w'T'$). The calculation methods for these variables are described in Sect. 2.3. The friction velocity serves as an indicator of the depth of the friction layer, and the covariance of the vertical velocity and temperature represents the strength of the thermally induced vertical mixing. Both variables were derived from observations 20 m onshore and *25* m offshore. The friction velocity was greater over the onshore site than over the offshore site from nighttime to daytime, indicating a thicker friction layer onshore (Fig. 14). Furthermore, the covariance of the vertical velocity and temperature onshore was low during the night but increased significantly to positive values during the day. In contrast, the diurnal variation offshore was small, with values remaining low throughout the day. These results suggest that the daytime friction layer over the offshore area was thinner than that over the onshore area. Therefore, when the wind direction shifts from a land breeze (nighttime to early morning) to a sea breeze (daytime) due to sea–land breeze circulation, the upper-level winds become decoupled from surface friction as the friction layer thins. This process leads to an increase in wind speed and a clockwise rotation of the wind direction, consistent with Blackadar's mechanism (1957). Although Blackadar's theory attributes stratification changes to nocturnal radiative cooling over land, the LLJs observed in this study are driven by wind direction

shifts associated with coastal sea–land breeze circulation. In addition, the occurrence of land–sea breeze circulation is closely related to the temperature difference between land and sea, and the formation of stable stratification over offshore areas during the daytime is favored in seasons when the sea surface temperature is lower than the land surface temperature. Konagaya et al. (2021) reported seasonal variations of sea surface temperature, onshore air temperature, and land surface temperature at the same site, indicating that such conditions are typically met from spring to summer. This is consistent with the higher occurrence rate of LLJs observed in this study during these seasons (Table 3). Although the conditions favorable for LLJ formation—namely land–sea breeze circulation and the development of stable stratification over offshore areas—are primarily satisfied from spring to summer, LLJs do not necessarily occur even during these seasons. Therefore, in addition to these factors, the occurrence of LLJs may be influenced by other factors, such as the strength of the land–sea thermal gradient and large-scale atmospheric conditions. However, in this study, no consistent relationship between these factors and LLJ occurrence was clearly identified. This remains a topic for future research.

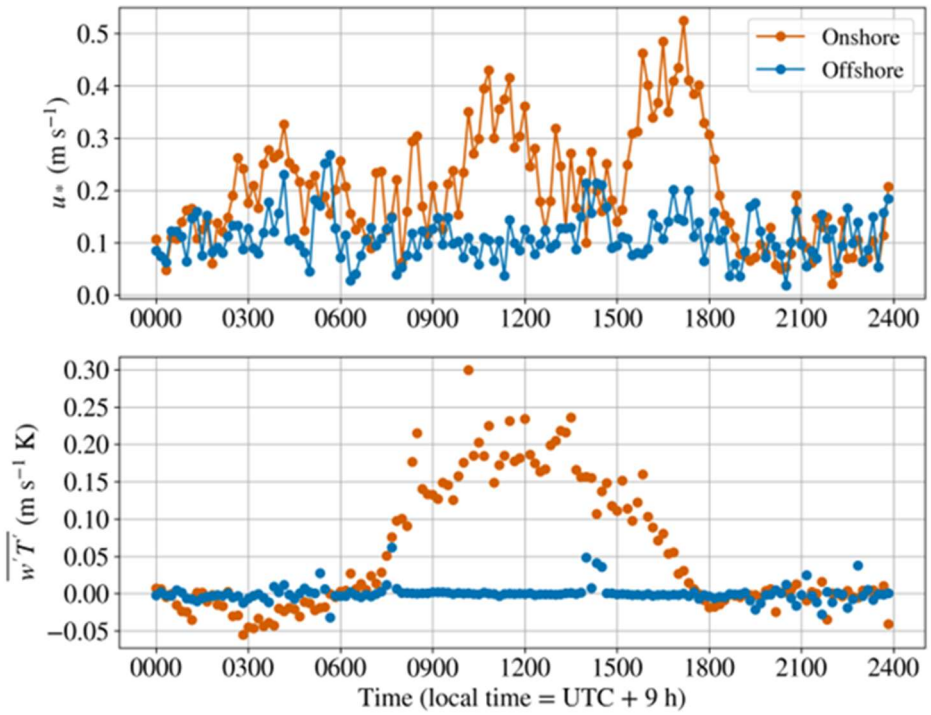

Figure 14: Time series of friction velocity and covariance of vertical velocity and temperature at the onshore and offshore sites on 2 May 2024

420

5 Conclusions

Wind behavior in Japan's coastal regions remains poorly understood. In this study, we aimed to elucidate this topic using LiDAR observational data obtained from both onshore and offshore installations. A comparison of wind speeds between onshore and offshore sites located 1.6 km apart indicated that nearby onshore data cannot directly substitute offshore wind
425 conditions near the coast. However, application of the MCP method to onshore data could facilitate such a substitution. Year-round observations revealed that the occurrence of LLJs strongly depends on wind direction, season, and time of day. The occurrence rate of LLJs by wind direction relative to all time periods was higher for winds parallel to the coastline, with southerly wind directions (SW–SE) showing approximately 12–29 % and northerly wind directions (N–NE) showing approximately 8–10 %, compared to other wind directions. In addition, the fraction of days with LLJ occurrences relative to
430 the total number of analyzed days was higher in spring and summer, with approximately 40 % in MAM and 37 % in JJA. Detailed analyses of individual LLJ cases suggest that wind direction changes associated with land–sea breeze circulation may contribute to the initiation of inertial oscillation. Specifically, transitions from land breeze to sea breeze during the day and

from sea breeze to land breeze at night may suppress vertical mixing and reduce the frictional influence on upper-layer winds, thereby facilitating the onset of inertial oscillation. As the inertial oscillation develops, wind speed tends to increase and the wind direction rotates clockwise under the influence of the Coriolis force. During this rotational process, LLJs are often observed, and this may explain the relatively higher occurrence of LLJs when the wind direction becomes aligned with the coastline.

These findings help develop wind-condition assessments, designs, and operational strategies for wind turbines that account for LLJs, and to develop LLJ forecasting methods for offshore wind energy projects. The maximum wind speed observed in LLJs was close to hub height; the wind speeds themselves were relatively modest compared to those reported in other countries. Therefore, further quantitative evaluation is required to assess the impact of LLJs on wind energy development in Japan. In addition, characterizing LLJ behavior at other locations remains an essential task for future research.

Code availability

The code used for the data analysis was developed by the authors and is not publicly available.

Data availability

The observational data used in this study were obtained from the Kobe University/NEDO Mutsu-Ogawara Offshore Wind Observation Site (https://mo-testsite.com/). The data are not freely available but can be purchased by anyone through the official website.

Author contribution

Kazutaka Goto conducted data curation, formal analysis, and visualization and contributed to the conceptualization, methodology, validation, and project administration. Takanori Uchida and Keisuke Nakao supervised the study and contributed to conceptualization, methodology, and project administration. Kazutaka Goto prepared the original draft, and all authors contributed to the review and editing of the manuscript.

Competing interests

The authors declare that they have no conflicts of interest.

Acknowledgements

We gratefully acknowledge the use of observational data from the Kobe University/MOC/NEDO Mutsu-Ogawara Offshore Wind Observation Site (https://mo-testsite.com/).

During the preparation of this work, the authors used ChatGPT in order to simplify expressions, correct typographical errors, adjust formatting, and check the English language. After using this tool, the authors reviewed and edited the content as needed and take full responsibility for the content of the publication.

References

Bailey, B. H., McDonald, S. L., Bernadett, D. W., Markus, M. J., and Elsholz, K. V.: Wind resource assessment handbook: fundamentals for conducting a successful monitoring program. AWS Scientific, Inc., Albany, NY, for National Renewable Energy Laboratory (NREL), Golden, CO, USA, National Renewable Energy Laboratory, Office of Energy Efficiency and Renewable Energy/SR-440-22223, 1997.

Blackadar, A. K.: Boundary layer wind maxima and their significance for the growth of nocturnal inversions, Bull. Am. Meteorol. Soc., 38, 283–290. https://doi.org/10.1175/1520-0477-38.5.283, 1957.

Carta, J. A., Velázquez, S., and Cabrera, P.: A review of measure-correlate-predict (MCP) methods used to estimate long-term wind characteristics at a target site, Renew. Sustain. Energy Rev., 27, 362–400. https://doi.org/10.1016/j.rser.2013.07.004, 2013.

de Jong, E., Quon, E., and Yellapantula, S.: Mechanisms of low-level jet formation in the U.S. mid-Atlantic offshore, J. Atmos. Sci., 81, 31–52. https://doi.org/10.1175/JAS-D-23-0079.1, 2024.

Debnath, M., Doubrawa, P., Optis, M., Hawbecker, P., and Bodini, N.: Extreme wind shear events in US offshore wind energy areas and the role of induced stratification, Wind Energ. Sci., 6, 1043–1059. https://doi.org/10.5194/wes-6-1043-2021, 2021.

Dörenkämper, M., Optis, M., Monahan, A., and Steinfeld, G.: On the offshore advection of boundary-layer structures and the influence on offshore wind conditions, Boundary Layer Meteorol., 155, 459–482. https://doi.org/10.1007/s10546-015-0008-x, 2015.

Emeis, S., Harris, M., and Banta, R. M.: Boundary-layer anemometry by optical remote sensing for wind energy applications, Meteorol. Z., 16, 337–347. https://doi.org/10.1127/0941-2948/2007/0225, 2007.

Goto, K., Uchida, T., Kishida, T., Nohara, D., Nakao, K., and Sato, A.: Investigating coastal effects on offshore wind conditions in Japan using unmanned aerial vehicles, Energies, 18, 1131. https://doi.org/10.3390/en18051131, 2025.

Grachev, A. A. and Fairall, C. W.: Dependence of the Monin–Obukhov stability parameter on the bulk Richardson number over the ocean, J. Appl. Meteorol., 36, 406–414. https://doi.org/10.1175/1520-0450(1997)036<0406:DOTMOS>2.0.CO;2, 1997.

Gryning, S. E., Batchvarova, E., Brümmer, B., Jørgensen, H., and Larsen, S.: On the extension of the wind profile over homogeneous terrain beyond the surface boundary layer, Boundary Layer Meteorol., 124, 251–268. https://doi.org/10.1007/s10546-007-9166-9, 2007.

Hallgren, C., Aird, J. A., Ivanell, S., Körnich, H., Barthelmie, R. J., Pryor, S. C., and Sahlée, E.: Brief communication: on the definition of the low-level jet, Wind Energ. Sci., 8, 1651–1658. https://doi.org/10.5194/wes-8-1651-2023, 2023.

Holton, J. R.: The diurnal boundary layer wind oscillation above sloping terrain, Tellus, 19, 199–205. https://doi.org/10.1111/j.2153-3490.1967.tb01473.x, 1967.

IEA and Wind, T. C. P.: Annual report 2022. International energy agency wind technology collaboration programme (IEA wind TCP), Paris, France, 2022. https://iea-wind.org/portfolio-item/annual-report-2022/.

Konagaya, M., Ohsawa, T., Inoue, T., Mito, T., Kato, H., and Kawamoto, K.: Land–sea contrast of nearshore wind conditions: case study in Mutsu-Ogawara, Sola, 17, 234–238. https://doi.org/10.2151/sola.2021-041, 2021.

Lundquist, J. K.: Wind shear and wind veer effects on wind turbines, in: Handbook of wind energy aerodynamics, edited by Stoevesandt, B., Schepers, G., Fuglsang, P., and Sun, Y., Springer, Cham, 859–880, 2022. https://doi.org/10.1007/978-3-030-31307-4_44.

New Energy and Industrial Technology Development Organization (NEDO): Offshore wind measurement guidebook, 2023. https://www.nedo.go.jp/content/100962731.pdf, Last accessed: 6 June 2025.

Porté-Agel, F., Bastankhah, M., and Shamsoddin, S.: Wind-turbine and wind-farm flows: a review, Boundary Layer Meteorol., 174, 1–59. https://doi.org/10.1007/s10546-019-00473-0, 2020.

Qiu, Z., Xian, J., Yang, Y., Lu, C., Yang, H., Hu, Y., Sun, J., and Zhang, C.: Characteristics of coastal low-level jets in the boundary layer of the Pearl River Estuary, J. Mar. Sci. Eng., 11, 1128. https://doi.org/10.3390/jmse11061128, 2023.

Renewable Energy Institute: Offshore wind power to support Japan's energy needs, 2021. https://www.renewable-ei.org/en/activities/reports/20210329.php, Last accessed: 6 June 2025.

Schulz-Stellenfleth, J., Emeis, S., Dörenkämper, M., Bange, J., Cañadillas, B., Neumann, T., Schneemann, J., Weber, I., zum Berge, K., Platis, A., Djath, B., Gottschall, J., Vollmer, L., Rausch, T., Barekzai, M., Hammel, J., Steinfeld, G., and Lampert, A.: Coastal impacts on offshore wind farms—a review focussing on the German Bight area, Meteorol. Z., 31, 289–315. https://doi.org/10.1127/metz/2022/1109, 2022.

Shimada, S., Takeyama, Y., Kogaki, T., Ohsawa, T., and Nakamura, S.: Investigation of the fetch effect using onshore and offshore vertical LiDAR devices, Remote Sens., 10, 1408. https://doi.org/10.3390/rs10091408, 2018.

Si, G., Xia, T., Wang, D., Gebraeel, N., Pan, E., and Xi, L.: Maintenance scheduling and vessel routing for offshore wind farms with multiple ports considering day-ahead wind-wave predictions, Appl. Energy, 379, 124915. https://doi.org/10.1016/j.apenergy.2024.124915, 2025.

Soares, P. M. M., Cardoso, R. M., Semedo, Á., Chinita, M. J., and Ranjha, R.: Climatology of the Iberia coastal low-level wind jet: weather research forecasting model high-resolution results, Tellus A, 66, 22377. https://doi.org/10.3402/tellusa.v66.22377, 2022.

Stull, R. B.: An introduction to boundary layer meteorology, Springer, Dordrecht. https://doi.org/10.1007/978-94-009-3027-8, 1988.

Svensson, N., Bergström, H., Sahlée, E., and Rutgersson, A.: Stable atmospheric conditions over the Baltic Sea: model evaluation and climatology, Boreal Environ. Res., 21, 387–404, 2016.

Taylor, P. A.: On wind and shear stress profiles above a change in surface roughness, Q. J. R. Meteorol. Soc., 95, 77–91. https://doi.org/10.1002/qj.49709540306, 1969.

Wagner, D., Steinfeld, G., Witha, B., Wurps, H., and Reuder, J.: Low level jets over the southern North Sea, Meteorol. Z., 28, 389–415. https://doi.org/10.1127/metz/2019/0948, 2019.

Ward, K. R., Bamisile, O., Ejiyi, C. J., and Staffell, I.: Time-averaged wind power data hides variability critical to renewables integration, Energy Strategy Rev., 50, 101235. https://doi.org/10.1016/j.esr.2023.101235, 2023.

Wetterdienst, D. (DWD), The FINO-WIND Project, n.d. https://www.dwd.de/EN/research/projects/fino_wind/fino_wind_en_node.html, Last accessed: 6 June 2025.

Wilczak, J. M., Oncley, S. P., and Stage, S. A.: Sonic anemometer tilt correction algorithms, Boundary Layer Meteorol., 99, 127–150. https://doi.org/10.1023/A:1018966204465, 2001.

Zecca, A. and Chiari, L.: Fossil-fuel constraints on global warming, Energy Policy, 38, 1–3. https://doi.org/10.1016/j.enpol.2009.06.068, 2010.